J Mater Sci: Mater Electron (2017) 28:10298–10312
DOI 10.1007/s10854-017-6798-5

CrossMark

IR studies of the oxygen and carbon precipitation processes in electron irradiated tin-doped silicon

E. N. Sgourou[1] · T. Angeletos[1] · A. Chroneos[2,3] · C. A. Londos[1]

Received: 1 March 2017 / Accepted: 20 March 2017 / Published online: 7 April 2017
© The Author(s) 2017. This article is an open access publication

Abstract Oxygen (O) and carbon (C) are key impurities in silicon (Si) and the control of their properties and behavior is an important issue for the microelectronic industry. A number of these properties can be manipulated by isovalent doping. Here we employ Fourier transform infrared (FTIR) spectroscopy to study the evolution of O and C concentration as well as the evolution of the oxygen precipitate bands in electron- irradiated tin (Sn) doped Si, subjected to isochronal anneals up to 950 °C. Special attention was given in connecting infrared absorption bands with certain precipitation morphologies. In this study, bands at 1040, 1060, 1080 and 1170 cm^{-1} generally attributed to precipitate morphologies were detected. Using arguments from classical theoretical mechanics we have attributed the 1040 cm^{-1} band to a structure more close to a spherical morphology, although the 1060 and 1080 cm^{-1} bands were attributed to structures more close to octahedral and polyhedral morphologies, respectively. Additionally the band at 1170 cm^{-1} was attributed to platelet precipitates. The effect of C and (C, Sn) co-doping Si in the morphologies of the precipitates bands was investigated in detail. It was found that in the irradiated material C suppresses the formation of spheroidal precipitates although it enhances the platelet precipitates, whereas in Si containing C and Sn the opposite behavior was detected. The presence of the two impurities modifies the number of the O precipitates and affects the relative density among the formed morphologies in Si, determining whether the spheroidal or platelet precipitates will prevail. The phenomenon was discussed taking into consideration the effect of the density of the nucleation sites on the interfacial energy of the precipitates. Furthermore, an inverse annealing stage in the evolution curve of C, namely an increase of C concentration prior to its complete disappearance was studied. This recovery stage was determined to be enhanced in (C, Sn) co-doping Si with relatively low Sn content although in Si with high Sn content the increase of C is substantially lower. An explanation was suggested based on the ability of the Sn to temporarily trap vacancies, thus affecting the restoration of the C substitutional atoms in the Si lattice.

✉ A. Chroneos
ab8104@coventry.ac.uk

C. A. Londos
hlontos@phys.uoa.gr

1 Solid State Physics Section, University of Athens, Panepistimiopolis Zografos, 157 84 Athens, Greece

2 Department of Materials, Imperial College London, London SW7 2AZ, UK

3 Faculty of Engineering, Environment and Computing, Coventry University, Priory Street, Coventry CV1 5FB, UK

1 Introduction

Si remains a mainstram semiconductor material for numerous nanoelectronic, sensor and photovoltaic devices [1–4]. The miniaturization of devices constitutes defect processes very important as their detailed understanding may influence material and/or device properties [5–8]. In particular during the manufacturing of devices thermal annealing, irradiation and doping are among the most usual technological processes of Si, however, they unavoidably introduce defects. Anneals at high temperatures result in precipitates [9–14] of the O and C impurities, which are unintentionally introduced during growth in the Si lattice. Additionally, irradiations introduce defect complexes formed from reactions between primary defects [vacancies (V) and self-interstitials (Si_I)] and

the O and C impurities, including divacancies, oxygen-vacancy and oxygen-carbon complexes [9, 12, 15]. There are interactions between the two kinds of defects and in particular radiation defects usually affect the growth and evolution of precipitates [16, 17].

Precipitates and radiation defects influence the yield and the performance of the Si-based devices. Their control and engineering is of importance both from a technological perspective (to improve the output of devices) and for scientific purposes (gain a better understanding of Si). To this end, isovalent doping is a widely used way to modify the Si material properties. Isovalent impurities (such as Sn) when introduced in the Si lattice occupy lattice sites and although they have limited effect on the electrical properties, they can modify the physicochemical behavior of the material as a result of the generation of elastic stresses in the lattice. Their presence can have significant consequences [18–26] on the Si properties and behavior in general. They can enhance the mechanical strength of the material and affect the carrier's mobility offering possibilities for bandgap engineering. Due to the difference of the covalent radius of the isovalent atom with the Si atom there are also possibilities for lattice parameter engineering. They can affect the micro-defect population enhancing the thermal stability of the material and also improve its radiation hardness. Additionally, they can interact with V and/or Si_I affecting their concentrations, which is an important factor during the various processing stages of Si. Moreover, they have a strong impact on the formation of V and Si_I related defects, due to the induced strains in the lattice. Key is the influence of isovalent dopants on the formation of O and C precipitates which impacts the fabrication of modern Si-based electronic devices.

O is an electrically neutral impurity inevitably incorporated during growth in the Si lattice at interstitial sites. In the course of thermal treatments at elevated temperatures supersaturated oxygen impurities tend to aggregate leading to the formation of SiO_x precipitates [10, 11]. Oxide precipitates can have positive but also negative effects in the functionality of devices [26–31]. Indeed they may be beneficial by acting as sinks for detrimental metallic impurities (internal gettering) and also can enhance the mechanical strength and stability of Si wafers by preventing dislocation movement. Additionally, they may act in conjunction with surrounding defects, as recombination centers reducing the efficiency of the corresponding devices. Depending upon the thermal history of the material and the temperature of the thermal treatments O precipitates have different forms and morphologies [10, 11] giving rise to a number of IR bands [32–34] in the spectral region of 1000–1300 cm^{-1}, around the strong IR band of oxygen at 1107 cm^{-1}. Notably, the formation of SiO_x precipitates is accompanied by a volume increase, which induces compressive strains in the Si lattice. One way that these strains may be relieved is by the emission of Si_I.

C is an isovalent impurity incorporated in the Si lattice at substitutional sites and is electrically inactive. On thermal treatments of Si at elevated temperatures if the C concentration is above its solubility limit it tends [12, 14, 35] to precipitate leading to the formation of silicon carbide (SiC) or alternatively to the formation of loose C–Si aggregates. Both processes lead to a volume reduction and are accompanied by the absorption of Si_I. Since the process of O precipitation is accompanied by the emission of Si_I, the simultaneous presence of O and C in the Si lattice relieves the strains facilitating the coprecipitation of both impurities. The effect of C on O agglomeration process is a complex issue and is investigated by the community due to its important technological interest [35–39]. In the present study, we used C-rich samples as well as samples co-doped with C and Sn in an attempt to investigate the impact of C and Sn isovalent doping on the oxygen aggregation and the impact of Sn on O and C aggregation in irradiated Si.

Irradiations or/and implantations are quite usually employed in conjunction with thermal treatments in device fabrication processes. However, the formation of irradiation induced defects in Si involves reactions with V and Si_I. Thus, defects such as VO, C_iO_i, C_iC_s, and on anneals V_nO_m and $C_iO_iSi_I$ clusters [9, 12, 40–44] affect the production and the balance of the V and the Si_I's concentrations. Since these primary defects play important role in O and C aggregation processes [9–14, 45–48] it is necessary to study such processes in irradiated material. Notably, VO and VO_2 defects have been suggested [49] to act as nucleation sites for O precipitation.

As we mentioned above, doping with isovalent impurities is a judicious choice to control and improve the quality of Cz-Si material for device fabrication. Sn doping is also important for the Si material properties. As Sn is larger than Si it readily attracts V and this reduces the formation of VO and VO_2 defects [50–52]. Additionally, Sn suppresses the formation of C-related defects [51] verifying the results of previously reported photoluminescence studies [28, 53]. In this framework Sn doping has been suggested as a way to enhance the radiation hardness of Si especially for applications related with solar cells and detectors operating in radiation environments [54, 55]. Additionally, since Sn attracts V and C binds with Si_I, Si codoping with Sn and C has been proposed [50] to further increase its radiation hardness and may be used as a tool to assess the degradation of Si-based devices. Furthermore, the presence of Sn significantly affects the formation of thermal donors and O precipitates formed on thermal treatments at elevated temperatures [28, 56–60].

In the present study we used FTIR spectroscopy to explore the effect of Sn isovalent doping on the evolution

of O and C impurities in carbon-rich Cz-Si subjected to electron irradiation and subsequent isochronal anneals up to 950 °C. Considering co-doping pairs (C, Sn) in Si will help us gain a more complete understanding of mechanisms that govern O and C precipitation processes as well as the ways that Sn isovalent dopants affect these processes. Importantly, since V and Si_I play [61–67] a key role in the O and C precipitation processes we can reversibly deepen our understanding on the mechanisms through which these primary defects affect the agglomeration of O and C impurities in Si treated at elevated temperatures. Also it could enhance the opportunities for technological improvements of Si providing an engineering strategy for thermal defects that could be employable to analogous systems. Isovalent dopants due to their larger size introduce stains in the Si lattice which affect the O and C aggregation processes. Notably, the application of high hydrostatic stress has been determined [68, 69] to have also a significant effect on the O agglomeration processes and comparison of the relative results would enhance our understanding of the two phenomena.

2 Experimental methodology

Samples used in the present study were cut from prepolished Cz-Si wafers with dimensions $10\times15\times2$ mm^3 and contained C. Besides a sample labeled Cz-Si with a low amount of C and a sample labeled Cz-Si:C with high C content we also used other Cz-Si samples contained carbon and doped with Sn (labeled respectively as Cz-Si:C,Sn_L and Cz-Si:C,Sn_H). The oxygen (1107 cm^{-1}) and carbon (605 cm^{-1}) concentrations were calculated by infrared spectroscopy using calibration coefficients [10, 12] 3.14×10^{17} cm^{-2} and 1.0×10^{17} cm^{-2}, respectively. The concentrations of the isovalent dopants in the samples were measured by secondary ion mass spectrometry (SIMS) and the values were given by the supplier's certificate. The samples were irradiated with 2 MeV electrons with a fluence of 1×10^{18} cm^{-2}, at ~70 °C, using the Dynamitron accelerator at Takasaki-JAERI (Japan). Information regarding impurities concentrations is given in Table 1. Notably, the O and C concentrations in the Cz-Si:C,Sn_H after the irradiation were higher than prior to irradiation. The increase of C was attributed [70] to the existence of Sn_sC_s complexes in the Si lattice, as a result of the growth procedure, which in the course of irradiation transform to Sn_sC_i complexes by reacting with Si_I ($Sn_sC_s + Si_I \rightarrow Sn_sC_i$). The Sn_sC_i defect is unstable at the temperature of irradiation and breaks to its constituent defects ($Sn_sC_i \rightarrow Sn_s + C_i$). Then C_i being mobile at these temperatures transform to C_s ($C_i \rightarrow C_s + Si_I$) resulting to the increase of C_s. Additionally, the observed increase of O_i after the irradiation can be attributed [70] in the presence of Sn_sO_i complexes in the Si lattice which as a result of irradiation lead to the release of more O_i atoms through the reactions ($Sn_sO_i + Si_I \rightarrow Sn_iO_i$ and $Sn_iO_i \rightarrow Sn_i + O_i$) resulting finally to the increase of the O_i. In the case of the sample Cz-Si:C,Sn_L with low Sn, only the O concentration was observed to increase after the irradiation. Seemingly, the release of C atoms from pre-existed Sn_sC_s complexes in this sample is not enough to cover the loss of C due to the formation of C_iO_i and C_iC_s defects as a result of the irradiation, so that overall the final C concentration is lower than that prior to irradiation.

After the irradiation, all the samples were subjected to 20 min isochronal anneals up to 950 °C in open furnaces with a step of ~10 °C. Following every annealing step, the IR spectra were recorded at room temperature using an FTIR spectrometer (JASCO-470 plus) with a resolution of 1 cm^{-1}. The two phonon background absorption was subtracted from each spectrum by using a float-zone sample of equal thickness.

3 Results and discussion

As a result of the thermal anneals the shape of the O band at 1107 cm^{-1}, as the temperature increases, becomes distorted due to the presence of other bands emerging in the spectra in the same frequency range and originating from O precipitates [11–13, 71]. The contribution of each individual precipitate band to the total signal can be recovered by making computer deconvolution using Lorentzian profiles.

Table 1 Information of the samples used in this work

Sample name	[Sn]($10^{18}cm^{-3}$)	$[C_s]_o$($10^{17}cm^{-3}$)	$[C_s]_{a.i.}$ ($10^{17}cm^{-3}$)	$[O_i]_o$ ($10^{17}cm^{-3}$)	$[O_i]_{a.i.}$ ($10^{17}cm^{-3}$)	$[C_s]_{max}$ ($10^{17}cm^{-3}$)
Cz-Si	–	0.5	<0.2	9.5	8.8	–
Cz-Si:C	–	2.2	1.2	10.0	8.9	1.5
Cz-Si:C,Sn_L	0.3	4.7	2.5	9.6	10.7	3.7
Cz-Si:C,Sn_H	9.0	2.0	2.6	9.2	9.7	2.5

The concentrations of Sn as well as of O_i and C_s before (o) and after irradiation (a.i.) for the 2 MeV electron irradiation at a fluence of 1×10^{18} $e\cdot cm^{-2}$, at $T_{irr}\approx70$ °C. $[C]_{max}$ represents the maximum concentration of carbon in the course of the isochronal anneals sequence

Figure 1 is the Lorentzian deconvolution of the O band at 1107 cm^{-1} for characteristic temperatures of the annealing process for the Cz-Si (1(a)), Cz-Si:C (1(b)), Cz-Si:C,Sn_L (1(c)) and Cz-Si:C,Sn_H (1(d)) samples, respectively. The analysis shows the existence of five additional bands at around 1000, 1040, 1060, 1080 and 1170 cm^{-1}. Notably, the bands found by the above analysis of the Lorentzian deconvolution are physically meaningful since there is ample experimental evidence, from various measurements also at low temperature, that the bands are related with oxygen precipitate morphologies [11–13, 71–76]. Initially, we will discuss the origin of each particular band in an attempt

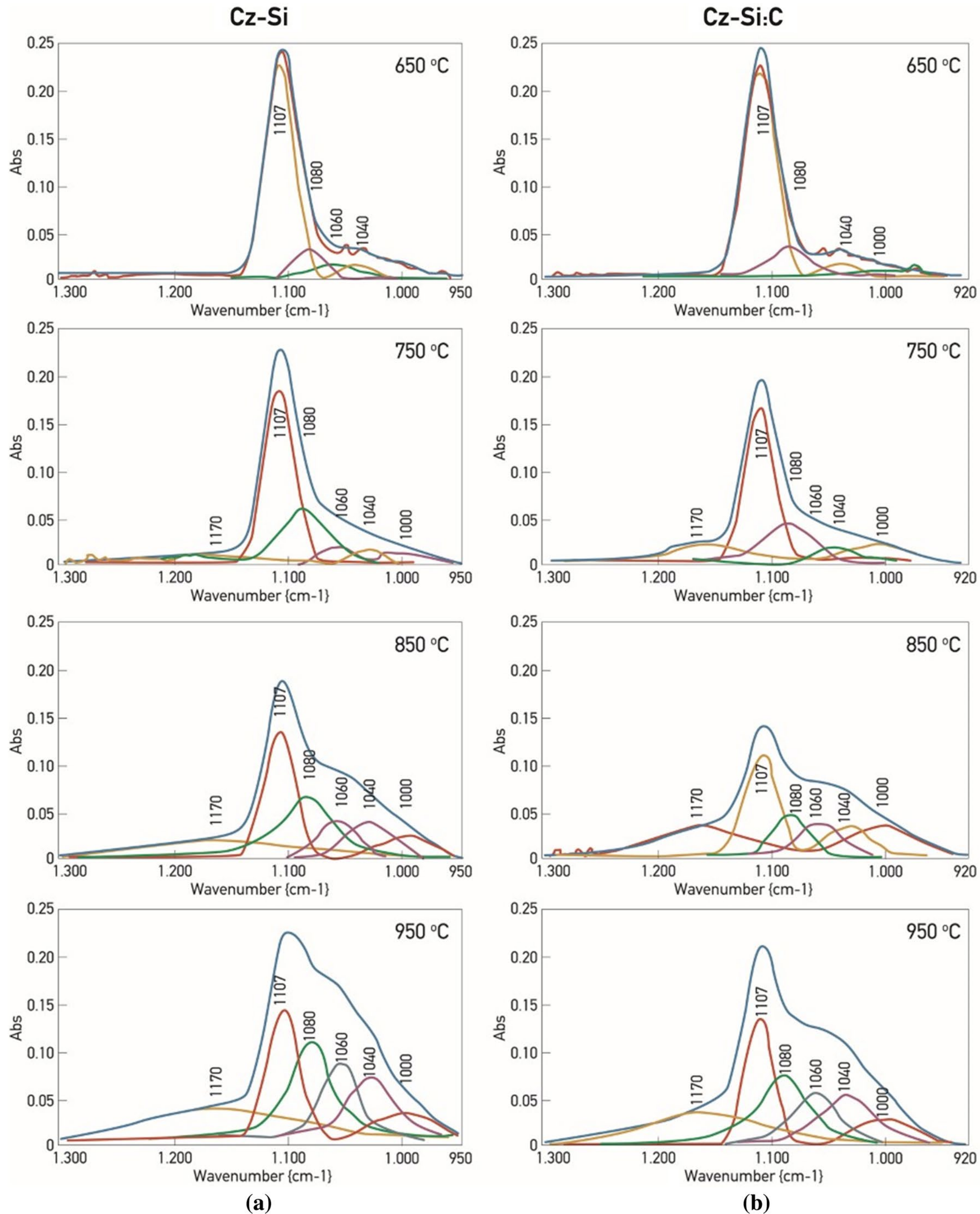

Fig. 1 Deconvolution of the IR band region around 1107 cm^{-1} (O_i) into Lorentzian profiles for the Cz-Si (**a**), the Cz-Si:C (**b**), the Cz-Si:C,Sn_L (**c**) and the Cz-Si:C,Sn_H (**d**) samples after irradiation at various characteristic temperatures in the course of the 20 min isochronal anneals sequence in the temperature range between RT and 950 °C

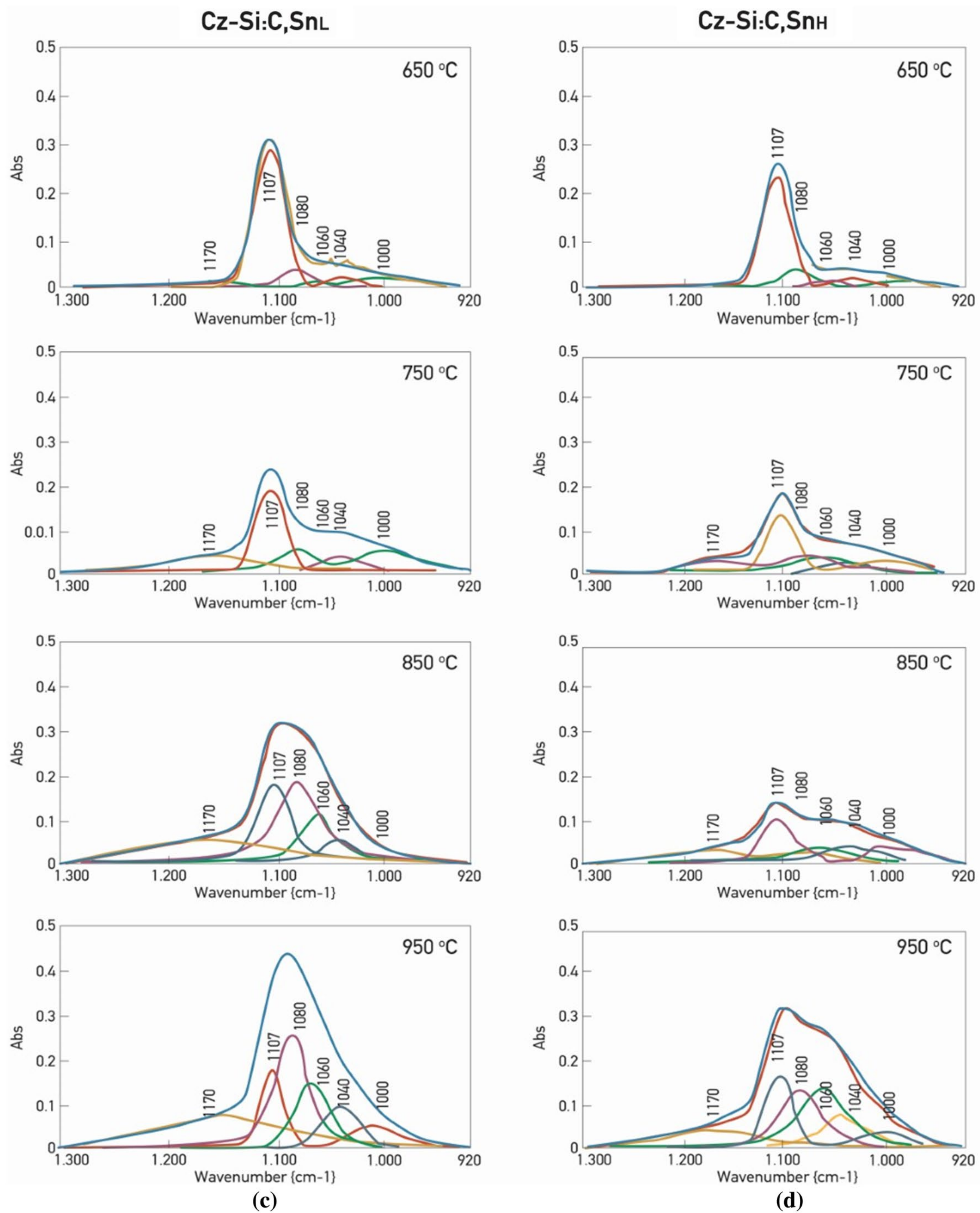

Fig. 1 (continued)

to correlate the absorption band frequencies with the shape and morphology of certain O precipitate structures.

A mathematical way to study the behavior of a precipitate is to consider its shape as an ellipsoid with three main axes (a_1, a_2, a_3). The various ratios of the main axes can properly describe all the possible common shapes of precipitates that is disc, sphere, and needle [72, 77, 78]. This shape mainly depends on the total free energy F of the structure, that is the sum of the strain and the surface (interfacial) energy [48, 79]. The smaller the size of a precipitate, the smaller the ratio of the strain energy to the surface energy. Obviously, as long as the size of the precipitate is small, the dominant energy term is the surface energy which favors in general a spheroidal morphology, since this

morphology minimizes this term. When the size of a precipitate increases, the dominant energy term is the strain energy which favors a platelet morphology. This morphology minimizes the ratio of the strain to the surface energy. Thus, platelet seems to be more favorable in comparison with spherical for the case of larger size precipitates [79].

In order to correlate the IR absorption spectroscopic profile of the small SiO_2 precipitates with their morphology, Hu employed [77] a model based on a theory of average dielectric function to describe the absorption in terms of polarization of the precipitate structure in Si. It was found that the IR band at 1230 cm^{-1} can be attributed to platelets [77]. In addition, Sassella et al. [72] assuming that the precipitate shape is modeled as a rotation ellipsoid with varying diameter/thickness ratio m (i.e. $m=1$ for spheres and $m>>1$ for thin discs) and applying effective medium theory (EMT) simulations showed that disc shaped precipitates gives a band around 1254 cm^{-1} while the spherical shaped precipitates are responsible [72] for a number of IR bands in the range of 1050–1150 cm^{-1}. Notably, the band at 1230 cm^{-1} is not present in our spectra. This point will be discussed in detail below. The determination of the elastic field of an ellipsoidal inclusion and its dependence on the shape of the related structure was thoroughly studied theoretically by Eshelby [80]. Using the results of this investigation, Voronkov [79] has calculated the critical value of the term P^2R, where R is the particle radius and P is the actual pressure created as a result of the induced strain due to the difference between the volume V_p of the non-strained particle and the volume V_c of the non-strained matrix cavity. One of the conclusions of this analysis was that the total free energy F of a spheroidal oxide precipitate depends on the aspect ratio α, namely the ratio of the smaller half axis c to the larger half axis a of the structure. Additionally, it was determined [81, 82] that the higher the annealing temperature (or the longer the annealing time, in the case of isochronal anneals) the larger the radius R of the precipitate and consequently the larger the pressure P of the structure. Figure 1a–d in Ref. 79 describe the changes of the curves of the total free energy of a precipitate structure in relation with the aspect ratio for four values of pressure P or equivalently for four respective values of annealing temperature. For example, Fig. 1a refers to a low value of P or annealing temperature, at an earlier stage of the precipitation process, although, Fig. 1d refers to a larger value of P or annealing temperature at a later stage of the process. By inspection of Fig. 1 one can observe that for low annealing temperatures (Fig. 1a) there is only one minimum of the total free energy characterized by a specific value of the curvature, which corresponds to the spherical morphology (α~1). As the temperature increases the total free energy curve gradually changes and a second local minimum (Fig. 1b), appears at a lower value of α (~0.4), corresponding generally to a spheroidal morphology. The position of this minimum shifts continuously to smaller values of α as the annealing temperature becomes larger (Fig. 1c) and the symmetry of the structure is lowered. The precipitate is gradually transformed to a more asymmetric structure (α~0.2), corresponding to platelet morphology. The minimum of the total free energy is now characterized by a larger value of curvature than that of the spherical (compare Fig. 1a, d).

From classical theoretical mechanics, at every stable equilibrium site (minimum of the energy vs. space coordinate diagram), for "small" displacements $\delta\alpha=(\alpha-\alpha_o)^2$ from the equilibrium position a_o, the potential curve can be approximated by a unique parabolic curve $U(a)=(1/2)\cdot k\cdot(a-a_o)^2$, where k stands for the term $[\partial^2U(\alpha\alpha)/\partial\alpha^2]\alpha_o$ which is proportional to the value of curvature of the potential curve at $a=a_o$. Accordingly, since the frequency ω is proportional to the square root of k, it is expected that the absorption band frequency of the platelet-shaped precipitates to be higher than that of the spheroidal-shaped. In general, a spheroidal morphology encompasses either spherical precipitates (structure with the higher symmetry), or octahedral precipitates (structure with lower symmetry) or polyhedral precipitates (structure with even lower symmetry). Taking the ratio of the absorption band frequencies called ω_{sph} and ω_{plat}, for the spheroidal and the platelet precipitate morphologies with masses M_{sph} and M_{plat} respectively, we have:

$$\left\{\left(\partial^2U(\alpha_o)/\partial\alpha^2\right)_{plat}/\left(\partial^2U(\alpha_o)/\partial\alpha^2\right)_{sph}\right\} = k_{plat}/k_{sph} = M_{plat}\omega_{plat}{}^2/M_{sph}\omega_{sph}{}^2 \text{or} \quad \omega_{plat}/\omega_{sph} = \left[\left(M_{sph}/M_{plat}\right)\cdot\left\{\left(\partial^2U(\alpha_o)/\partial\alpha^2\right)_{plat}/\left(\partial^2U(\alpha_o)/\partial\alpha^2\right)_{sph}\right\}\right]^{1/2} \tag{1}$$

Considering again Fig. 1 of Ref. 79, the total free energy curve of an ellipsoid precipitate at the region of the total minimum was fitted with a polynomial function $f(x)=a_0+a_1x+a_2x^2+\mathcal{O}(x^3)$. The optimum fitting was reached by using a parabolic function ($a_n=0$ for $n\geq3$). At low annealing temperatures (refer to Fig. 1a) the size of the precipitate structure is small. At higher annealing temperatures (refer to Fig. 1b–d) the size of the precipitate is expected to increase gradually. Notably, the curvature of the minimum of the total free energy curve has a greater value in the case of Fig. 1d as compared to the minimum of the Fig. 1a. Additionally, the position of the minimum corresponds to a lower aspect ratio in the case of Fig. 1d. Furthermore, comparing spheroidal and platelet morphology precipitates (by fitting the curves in Fig. 1c, d) the corresponding parabolic functions are derived:

$$f_{sph}(x) = 654a^2 - 467a + 78,\ a_{o\,sph} = 0.35,\ \left[\partial^2U(\alpha_o)/\partial\alpha^2\right]_{sph} = 1308$$

$$f_{plat}(x) = 7183a^2 - 325a + 253,\ a_{o\,plat} = 0.23,\ \left[\partial^2U(\alpha_o)/\partial\alpha^2\right]_{plat} = 14366$$

where $f_{sph}(x)$ stands for spheroidal and $f_{plat}(x)$ for platelets.

Thus, from Eq. (1) we have:

$$\omega_{plat}/\ \omega_{sph} = 3.32 \cdot \left(M_{sph}/M_{plat}\right)^{1/2} \quad (2)$$

Now, we assume that the density of a spheroidal structure is not much different from that of a platelet structure since the bond length of SiO_2 unit is practically the same between the two morphologies. Notably, the difference of the actual pressure P in the oxide, between spheroidal and platelet structures is ~9% (compare Fig. 1c, d in Ref. 79). This change of P is shared between all the SiO_2 units in the precipitate structure and therefore the actual change of the bond length of a single SiO_2 unit is practically negligible. Thus, the ratio of the masses m_{plat}/m_{sph} could be taken approximately equal to the ratio of the volumes V_{plat}/V_{sph}. These volumes have been measured by transmission electron microscopy (TEM) [83–85] and calculated by using Ham's theory [86]. The corresponding values are $V_{sph} \approx 10\ \mathrm{nm}^3$ and $V_{plat} \approx 100\ \mathrm{nm}^3$ respectively, from which we receive $V_{sph}/V_{plat} \approx 0.1$. Replacing the above values of the volume ratio instead of the mass ratio in Eq. 2 we finally have:

$$\omega_{plat}/\ \omega_{sph} \approx 1.05 \quad (3)$$

A final comment regarding relation (2) deserves to be noted. It is known that for the case of molecules, the frequency is proportional to the inverse square root of the mass of the molecule. Our analysis shows that this relation could be extended also for the precipitate masses. This is reasonable given that the frequency of the precipitate morphology depends on both the size and the shape, and not on the chemical bonding of the structure [11, 87].

In the present experiment, Lorenzian profiling was employed in the region 950–1300 cm^{-1} around the 1107 cm^{-1} O band. IR bands at $\omega_1 = 1170$, $\omega_2 = 1080$, $\omega_3 = 1060$ and $\omega_4 = 1040\ \mathrm{cm}^{-1}$ were related to O precipitates [72–76]. Before proceeding with the identification of these bands, it is necessary to discuss the absence of the 1230 cm^{-1} band from our spectra. This band has been attributed [32, 71, 77, 87] to platelet-shaped precipitates. The structure becomes IR active only when its size is smaller than 0.36 μm and it is shifted towards lower wavenumbers when the precipitates structure becomes more spheroidal [77]. In agreement with the above, it has been reported [88] that a thin oblate spheroid (simplification of a platelet) with an aspect ratio~0.01 gives rise to an absorption band at 1227 cm^{-1}. The gradually change of the morphology from plate-like to more spheroidal shapes with larger aspect ratio shifts the frequency to lower wavenumbers [88]. Remarkably however, the 1230 cm^{-1} band has not been detected in the spectra in a number of previous experimental works [32, 37, 71, 87, 89–91]. It is important to note that the dominant factors that determine the morphology of a precipitate structure, are the thermal treatment process as well as the initial oxygen and carbon concentration of the Si material.

Regarding oxygen impurity, it has been determined [92] that the initial oxygen concentration of the sample plays a key role in defining the prevailing morphology of the formed precipitates. In particular, when this concentration is lower than a critical value, precipitates are mainly octahedral and/or polyhedral structures due to the very low oxygen supersaturation. No platelet precipitates can be formed under these conditions [92]. In agreement with this, it has been reported [32] that on samples submitted to thermal treatments, the 1230 cm^{-1} band of platelets appears in the spectra of high oxygen concentration samples, although in two samples of low oxygen concentration the band is absent.

Regarding thermal treatments, it has been observed [11, 87, 89, 93–97] that when the samples were subjected to long term pre-annealing treatments at low temperatures [11, 87–89, 93–95] i.e. at ~750 °C or even lower temperatures [37, 90, 96] i.e. at ~450-650 °C an emission of a large amount of Si_I takes places and rod-like defects are formed [90]. On further anneals at higher temperatures these defects act preferentially as nuclei for oxygen impurities to precipitate [90] rather than forming new platelets precipitates or precipitating on already existing platelets. In essence, this two-step annealing sequence leads to a suppression of platelet precipitate formation [90]. Additionally, it was found [90] that in the case of long term pre-annealing treatments at low temperatures, the size and density of rod-like defects increases. At higher temperature anneals these rod-like defects are converted into stacking faults relieving the platelet suppression [11, 87, 90]. However, at these higher temperatures firstly no more sufficient nucleation of oxygen precipitates occur and secondly some already existing small precipitate nuclei disappear [90]. In essence, no platelets form under these circumstances. Admittedly, for longer pre-annealing time durations, only large platelets which survived through the above suppression effect may exist [90]. If these structures however have size larger than 0.36 μm they do not give any absorption [77] at the 1230 cm^{-1}. Besides, any process initiated from small nuclei which survived from the shrinking or the coalescence effect [90] and could potentially lead to the formation of platelet-shaped precipitates at higher temperatures does not occur. Instead, these small nuclei prefer to transform into precipitate structures of higher aspect ratio or they dissolve and form microprecipitates [87, 90]. Significantly enough, a transition between plate-like morphologies and morphologies with larger aspect ratio, for instance octahedral, was previously determined [87, 91]. It is therefore concluded that the enhancement of the density

of microdefects, introduced by the low temperature pre-annealing treatments, creates the conditions for the suppression of platelets morphologies. Furthermore, in the case of high temperature pre-annealing treatment the formation of microdefects is not favorable and therefore platelets could be formed [96]. In summary, when the samples are subjected to low temperatures pre-annealing treatment followed by a high temperature thermal anneal, the 1230 cm^{-1} band is generally not detected.

Regarding carbon, previous works have shown [37, 89, 93–96] that in carbon-doped Cz-Si samples subjected to various heat treatments the 1230 cm^{-1} was not observed. Carbon presence suppresses the formation of large size oxygen precipitates and favors the formation of higher density precipitates but of smaller size [93]. There are two key points. In one hand carbon releases strains in the lattice and on the other hand platelet-shaped precipitates are stabilized only when the local strain is high. As a result, the presence of carbon forces platelet structures to transform [94] into polyhedral structures, which have generally a larger aspect ratio. Importantly, a band at ~1180 cm^{-1} has been attributed [71, 75, 76, 78] to platelet shaped precipitates.

In the present study, irradiated Cz-Si samples containing carbon were subjected to isochronal anneals starting from low temperatures ~100 up to ~950 °C. From the above analysis, it can be concluded that this isochronal annealing sequence could be simulated with a two-step thermal treatment where the first step occurs at relatively low T and the second step at relative high T. In agreement and with ref. 37 the 1230 cm^{-1} band is absent. Instead, a band at 1170 cm^{-1} found in our spectra is related to platelet morphologies [71, 75, 76, 78]. The latter band is considered to originate from a thin oblate spheroidal morphology, which approximates that of a platelet [71, 88]. Apparently, its aspect ratio is larger than that of the platelet precipitate morphology related with the 1230 cm^{-1} band.

Returning now to the analysis of our results, we have to state that all the evidence from various studies so far lead us to correlate the 1170 cm^{-1} band to platelet precipitates, although the 1060 and 1080 cm^{-1} bands to spheroidal precipitates [72–76]. The band at 1040 cm^{-1} is just outside the frequency range (1050–1150 cm^{-1}) where spheroidal precipitate bands appear [72]. Previous studies have correlated this band with dendritic or needle-like precipitates [73, 98, 99]. We shall discuss this issue in what follows. Furthermore, a band at 1000 cm^{-1} detected in our spectra, has not been correlated with any known precipitate morphology.

By considering Eq. 3 the corresponding ratio of frequencies, for the present experimentally detected bands, are $\omega_1/\omega_2 = 1.08$, $\omega_1/\omega_3 = 1.10$ and $\omega_1/\omega_4 = 1.13$. The theoretically received ratio $\omega_{plat}/\omega_{sph} = 1.05$ was produced by comparison of Fig. 1(c) and (d), of Ref. 79 and relates the frequency attributed to a platelet precipitate with the corresponding frequency of a spheroidal precipitate. It was previously suggested [71] that the higher the symmetry of a morphology, the lower the frequency of the related IR band or the larger the $\omega_{plat}/\omega_{sph}$ ratio. Thus, since the most symmetric shape among all the spheroidal morphologies is the spherical one, which has the lower frequency, it is more likely to connect the ratio $\omega_1/\omega_4 = 1.13$ and therefore the 1040 cm^{-1} band with a structure more close to a spherical morphology. Analogously, the ratio $\omega_1/\omega_3 = 1.10$ corresponds to a morphology with lower symmetry than that of 1040 cm^{-1}. To this end the 1060 cm^{-1} band could be attributed to a structure more close to an octahedral morphology. Similarly, $\omega_1/\omega_2 = 1.08$ corresponds to a morphology with even lower symmetry and, therefore, the 1080 cm^{-1} band could be attributed to a structure more close to a polyhedral morphology. Finally, regarding the 1000 cm^{-1} band detected in these studies it is not easy to make any assignment. At first, it has not been reported to the best of our knowledge any attribution of such a band to precipitates. Additionally, we notice that the absorption spectra of oxide precipitates in Si are expected to be located in the Reststrahlen region of the composite, which is between [100, 101] 1000 and 1300 cm^{-1}. Since the 1000 cm^{-1} value is at the lower limit of the Reststrahlen region it is not prudent to make any attribution and further experimental and theoretical work is necessary to resolve the origin of this band.

Figure 2 displays the variation with temperature of the O interstitial intensity (1107 cm^{-1}) for the Cz-Si, the Cz-Si:C, the Cz-Si:C,Sn_L and the Cz-Si:C,Sn_H samples as well as the variation of the O precipitation related bands. The purpose is threefold: Firstly, to monitor variations in the evolution of O in the course of the isochronal anneals, as a result of the presence of C in the Cz-Si:C in comparison with the Cz-Si. Secondly, to monitor the variations of O due the presence of C and Sn co-doping in the Cz-Si:C,Sn_L and the Cz-Si:C,Sn_H samples. Thirdly, to monitor the evolution of the O precipitate bands in the various samples.

Noticeably, after the irradiation the spectra of the samples contain various O and C related bands. The origin and the behavior of these bands have been studied in detail in our previous studies [102, 103] and will not be considered here. Regarding the evolution of the oxygen band we observe at first that in all the samples there are two stages of decrease as the annealing T increases. The first stage is in range from RT up to ~700 °C. In this first stage the decrease of the O concentration is slight but it is larger in the Cz-Si:C sample than that in the Cz-Si. It is even larger in the Cz-Si:C,Sn_L and the Cz-Si:C,Sn_H samples. This stage is certainly related with the formation and transformations of the various radiation defects formed in the course of irradiation (for instance VO and C_iO_i), which upon annealing give rise to larger clusters [102, 103]. Such clusters are, for instance, the various VO_n and generally

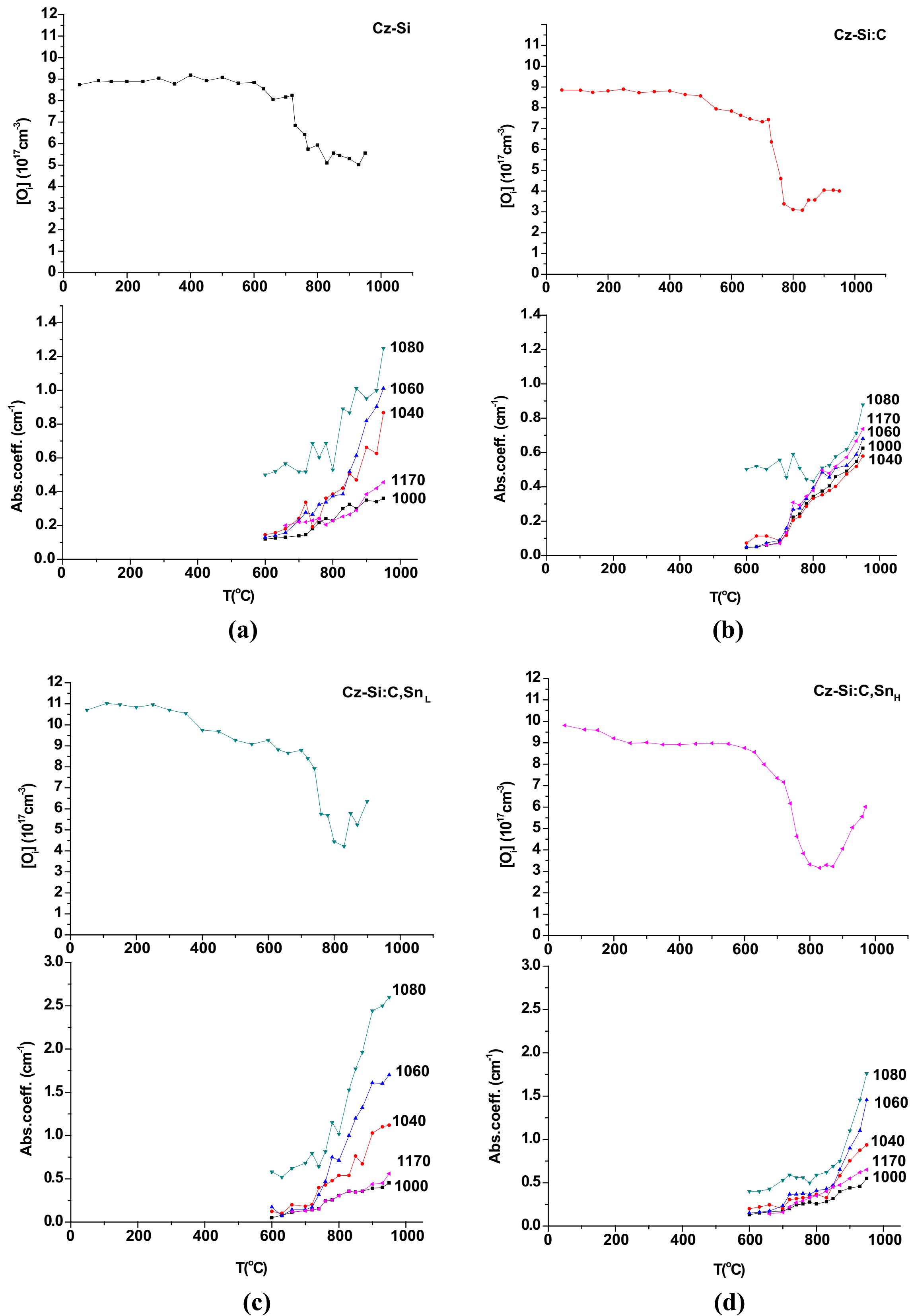

Fig. 2 The evolution with temperature of the oxygen interstitial band at 1107 cm^{-1}, as well as of the other IR bands at 1000, 1040, 1060, 1080 and 1170 cm^{-1} representing various oxygen precipitate morphologies for the Cz-Si (**a**), the Cz-Si:C (**b**), the Cz-Si:C,Sn_L (**c**) and the Cz-Si:C,Sn_H (**d**) samples, respectively

V_nO_m defects as well as carbon–oxygen related defects such as $C_iO_i(Si_I)_n$ centers. Additionally, at ~450 °C O atoms start to diffuse in the Si lattice and begin to aggregate [10, 104] forming initially thermal donors (TDs) and at a later temperature stage O precipitates. All these processes require the involvement of O, which is reflected in the decrease of O concentration. When C is present in the material also carbon–oxygen complexes form [105–107]. Additionally, we note that C enhances [108] the formation of the *V*O and generally of the VO_n defects. We also note that C suppress [11, 12] the formation of TDs. Apparently, the reduction in the O loss due to the suppressed formation of TDs does not compensate for the additional loss of O due to the enhanced formation of VO_n complexes and the production of carbon–oxygen defects. Thus, the decrease of O in this temperature range is found to be larger in the Cz-Si:C than that in the Cz-Si sample. This is expected due to the additional interaction between O and C in the first sample. In the case now of C and Sn co-doping, the presence of Sn makes the situation even more challenging. At first, we note that Sn generally suppresses [51, 109, 110] the formation of *V*O, VO_n as well as the formation C_iO_i and $C_iO_i(Si_I)_n$ defects. Secondly, Sn also suppress [111] the formation of TDs. Additionally, it has been reported [60, 111–114] the formation of Sn*V*O complexes as well as Sn–O pairs. Remarkably, it was suggested [60] that Sn–O pairs could serve as nucleation sites for heterogeneous precipitation of O impurities in Si. Considering all these reactions and processes that O participates, the O loss in C and Sn co-doping samples Cz-Si:C,Sn_L and Cz-Si:C,Sn_H is expected to be larger than that in the C doping Cz-Si:C sample, a fact verified in our studies (Fig. 2).

In the second stage, in the range between 700 and 800 °C a large decrease of O concentration is observed (Fig. 2). This decrease underlines the onset of the main precipitation process and it is manifested by the increase of the various precipitates bands discussed above. By comparing of the evolution curves of the Cz-Si and Cz-Si:C samples it is immediately observed that the total O loss at this temperature range is larger in the C contained sample. In order to discuss these observations we have to consider the simultaneous evolution of the precipitate bands. As it is immediately seen comparing Fig. 2a, b the strength of the precipitate bands is lower in the Cz-Si:C sample which at first sight is the opposite than that it was expected due to the greater loss of the O band in Si in the course of precipitation. Nevertheless, a larger loss of the interstitial O concentration does not necessarily imply an enhancement of the density of precipitates since the O content undergoes an additional reduction due to the formation of carbon–oxygen complexes [115] as for instance perturbed C_iO_i centers [116, 117]. The loss of O atoms to unknown sinks cannot be excluded. Furthermore, it has been argued [115] that in high C and O material co-precipitates of SiO_2 and SiC may exist. In that case, as C atoms participate in O complexes there is an excess of available Si_I which dissolve existing O precipitates resulting in their suppression [115]. Considering now the Sn-doped samples, we observe that the intensities of the spheroidal precipitate bands 1040, 1060 and 1080 cm^{-1} are generally stronger in these samples (Fig. 2c, d) than in the Cz-Si and Cz-Si:C samples (Fig. 2a, b). This can be better seen more clearly by another presentation of the results as in Fig. 3. This figure exhibits, for comparison purposes, the variation of the 1000 (a), 1040 (b), 1060 (c), 1080 (d) and 1170 cm^{-1} (e) bands respectively for the Cz-Si, the Cz-Si:C, the Cz-Si:C,Sn_L and the Cz-Si:C,Sn_H samples that is the evolution of each particular band for all the samples used in this work. A simple inspection shows that the O precipitate bands at 1040, 1060 and 1080 cm^{-1} related with spheroidal morphologies are of lower intensity in the Cz-Si:C sample in comparison with the Cz-Si, Cz-Si:C,Sn_L and Cz-Si:C,Sn_H samples. The opposite is observed for the case of the platelet precipitate band at 1170 cm^{-1}. Its intensity is higher in the Cz-Si:C sample than that in the Cz-Si:C,Sn_L and Cz-Si:C,Sn_H samples. The intensity is even lower in the Cz-Si sample.

At first we observe that in all the samples, both spheroidal and platelet precipitates are found in the spectra. O precipitation occurs [49, 118–122] either by homogeneous or/and heterogeneous nucleation. In the former case, aggregating O atoms serve as potential sites for nucleation through spherical precipitate nuclei, although in the latter case O precipitation occurs at heterogeneous sites at various impurities for instance here C and Sn, as well as point defect clusters for instance *V*O and VO_2 defects and some forms of O-C complexes [49, 116–122]. In general, homogeneous precipitation is expected to lead to spheroidal precipitates although heterogeneous precipitation to lead to platelet precipitates [118–121]. However, the situation is generally more complex, since homogeneous nucleation of platelet precipitates can also occurs [120]. It is therefore evident that in our sample both spheroidal and platelet precipitates are expected to form in the course of annealing of the irradiated material and this is verified in the IR spectra by the presence of bands related to these morphologies.

Let us now discuss our results within the above framework. In the case of the Cz-Si:C sample, the presence of carbon–oxygen centers besides the vacancy–oxygen centers in comparison with the Cz-Si sample, provides additional sites for inhomogeneous nucleation and therefore platelets are expected to have a larger density in this material. This is verified in the spectra by the greater intensity of the corresponding band at 1170 cm^{-1} (refer to Fig. 3e). In the case of the (C, Sn) co-doped samples the intensity of the platelets band is higher than that of the Cz-Si sample but lower than that of the Cz-Si:C sample. Indeed in these (C, Sn) co-doped

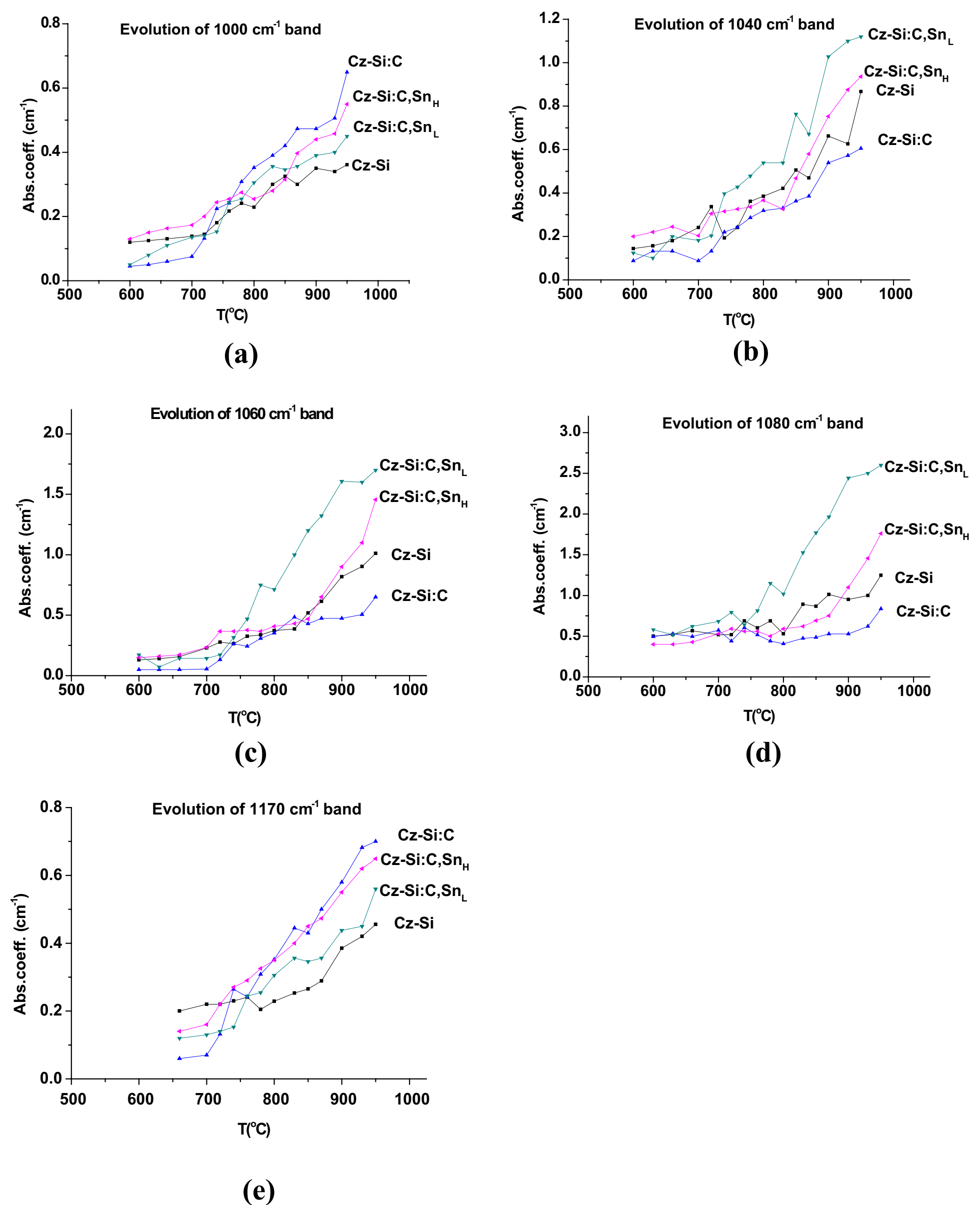

Fig. 3 The evolution with temperature of the oxygen precipitate bands at 1000 (**a**), 1040, (**b**) 1060 (**c**), 1080 (**d**) and 1170 cm^{-1} (**e**), respectively for the Cz_Si, the Cz-Si:C (**b**), the Cz-Si:C,Sn_L(**c**) and the Cz-Si:C,Sn_H (**d**) samples

samples the additional presence of Sn enhances the number of nucleation sites leading to the formation of more platelets than in the case of the Cz-Si sample. However, the intensity of the platelets band in lower in the (C, Sn) co-doped sample than in the Cz-Si:C sample. Notably, in previous studies [51, 109] we have reported that Sn suppresses the formation of *V*O, VO_2 and C_iO_i. pairs. In the case of Sn-doped samples subjected to thermal anneals it is suggested that the competition between O and Sn to capture *V* can lead to a reduction of the number of vacancies bonded to oxygen atoms to form vacancy-oxygen centers. These centers however provide [48, 49] nucleation sites mainly for heterogeneous nucleation. Their reduction is reflected in the lower intensity of the 1170 cm^{-1} band of platelets in the (C, Sn) co-doped samples in comparison with the Cz-Si:C sample. In the case now of the spheroidal precipitate bands at 1040, 1060 and 1080 cm^{-1} mainly formed through a homogeneous nucleation process, their intensity is clearly lower for the Cz-Si:C sample as compared to the Cz-Si sample (Fig. 3b–d). It has been reported [75] that the amount of spheroidal precipitates is about four times larger than that of the platelet precipitates. Since in the Cz-Si:C sample the O loss is mainly directed to the formation of platelets, the intensity of the spheroidal bands is lower than that of the Cz-Si sample as observed in Fig. 3b–d. In the case now of the (C, Sn) co-doped samples both impurities provide nucleation sites which lead [123] to higher precipitate density. In that case the favored morphology is that of a spheroidal precipitate which has a lower interfacial energy than that of a platelet and therefore a lower total free energy [11, 79]. Therefore, the intensities of the spheroidal bands are expected

to be larger in these samples in agreement with the present study. Furthermore we notice that the intensities of the 1040, 1060 and 1080 cm^{-1} bands are lower in the Cz-Si:C,Sn_H than in the Cz-Si:C,Sn_L sample. This trend is the opposite than that displayed by the platelet precipitate band 1170 cm^{-1} where its intensity is higher in the Cz-Si:(C,Sn_H) sample. In a first approximation, it may be argued that Sn induces larger strains in the Si lattice of the Cz-Si:Sn_H sample than that of the Cz-Si:Sn_L sample. It is well established [124] that the smaller the aspect ratio of a precipitate ellipsoid structure, the smaller the strain energy. Thus, the morphology of the platelets precipitates is more favorable to form in the Cz-Si:(C,Sn_H) sample in order to decrease the induced strain energy. Correspondingly, the spheroidal morphology is less favorable. This is reflected in our results by the larger intensity of the platelet precipitates and the smaller one of the spheroidal in the case of Cz-Si:C,Sn_H sample in comparison with the Cz-Si:C,Sn_L sample. The total number of O atoms which participate in the precipitation would lead to the formation of both platelets and spheroidal morphologies. Thus, it is expected that when the intensities of the spheroidal morphologies are enhanced then the intensities of the platelets morphologies for the same sample are suppressed, as observed in Fig. 2c, d.

Figure 4 displays the variation with temperature of the intensity of the C substitutional band (605 cm^{-1}) for the Cz-Si:C, the Cz-Si:C,Sn_L and the Cz-Si:C,Sn_H samples. A simple inspection shows that in the temperature region of ~500 to ~700 °C, in the course of anneal, the intensity of the C substitutional band increases gradually and this is an indication of the release of carbon atoms. The phenomenon was also observed previously [125] in irradiated Ge-doped Si and was connected with the supersaturation of Si_I's. In particular, the recovery of C substitutional atoms observed in the spectra by the increase of the intensity of the 605 cm^{-1} was connected with the formation of $C_N(Si_I)_M$ complexes. These complexes act [66] as sources of these additional C atoms either involved in reactions with Si_I's and V or/and transformed to SiC precipitates. Notably, C and Si_I clustering leading in general to the formation of $C_N(Si_I)_M$ complexes has been extensively discussed in the literature [66, 126, 127]. In particular, it was suggested [66] that upon increasing the annealing temperature, various reactions take place involving V, Si_I as well as C_s and C_i leading to the formation of $C_N(Si_I)_M$ complexes. Sources of V are possibly large vacancy clusters [128, 129] and sources of Si_I's are possibly large self-interstitial clusters [130, 131] present in Si, as a result of anneals. In the case of Cz-Si:C sample the following sequential reactions are envisaged [66] to take place:

$$V + Si_I \rightarrow \varnothing \quad (4)$$

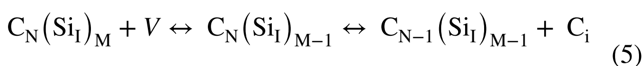

$$C_N(Si_I)_M + V \leftrightarrow C_N(Si_I)_{M-1} \leftrightarrow C_{N-1}(Si_I)_{M-1} + C_i \quad (5)$$

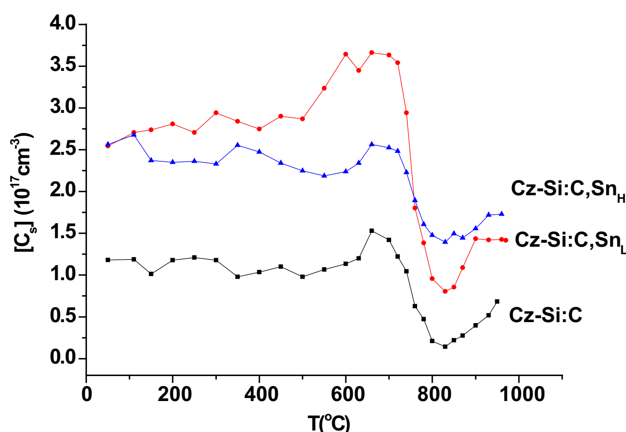

Fig. 4 The evolution with temperature of the carbon substitutional band at 605 cm^{-1}, for the Cz-Si:C, the Cz-Si:C,Sn_L and the Cz-Si:C,Sn_H samples, respectively

$$C_i + V \leftrightarrow C_s \quad (6)$$

We assume that a number of V survives annihilation according to reaction (4) and these vacancies participate in reactions (5) and (6). Reaction kinetics theory impose [132] that due to the provision of these additional V the equilibrium of the latter reactions shifts in the forward direction. The additional carbon atoms liberated in this way (reactions 5, 6) contribute to the observed increase of the 605 cm^{-1} band in the Cz-Si:C sample. In the case of the Cz-Si:C,Sn_L sample it is observed that the increase of C_s is larger than that of the Cz-Si:C sample (Fig. 4). This increase could be understood by considering that the presence of Sn atoms in the Si lattice suppresses the annihilation rate of V and Si_I's in the following way. A fraction of the V is temporarily captured by Sn atoms forming SnV centers which at these temperatures act as transient species. These V do not participate in the annihilation reaction (4), which is therefore retarded. The subsequent release of the V from the temporarily formed SnV pairs is then expected to enhance reaction (6). Thus, a larger number of C_s is produced, reflected to the observed increase of the 605 cm^{-1} band. In the case now of the Cz-Si:C,Sn_H sample the increase of C_s is observed to be substantially lower than that of the Cz-Si:C,Sn_L sample (Fig. 4). It can be postulated that when the Sn concentration is particular high, the binding energy of the SnV transient species is affected as a result of the enhanced strains induced by the Sn atoms in the Si lattice. This leads to an increase of the survival lifetime of the SnV pairs, which in turn leads practically to an increase of the availability of the Si_I atoms. In this case the corresponding scheme of reactions that govern the phenomenon is:

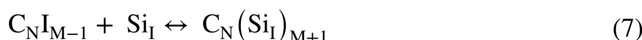

$$C_N I_{M-1} + Si_I \leftrightarrow C_N(Si_I)_{M+1} \quad (7)$$

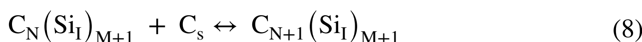

$$C_N(Si_I)_{M+1} + C_s \leftrightarrow C_{N+1}(Si_I)_{M+1} \quad (8)$$

Thus the increase of C_s in Cz-Si:C,Sn_H sample is lower than that of the Cz-Si:C,Sn_L sample. In addition, in the case of Cz-Si:C,Sn_H sample, some of the C_s atoms may be captured by Sn to form Sn_sC_s defects as those existed in the Cz-Si:C,Sn_H sample prior to the irradiation and described in Sect. II.

4 Conclusions

FTIR spectroscopy was employed to investigate the impact of Sn doping on the evolution of O and C impurities in irradiated Si. Moreover we studied the effect of C as well as the effect of the (C, Sn) co-doping on the evolution of the O precipitates IR bands in the course of isochronal anneals up to 950 °C. By fitting the total free energy curve of a precipitate structure in relation with its aspect ratio it was determined that the more asymmetric the structure, the larger the frequency of the corresponding absorption band, confirming previous reports. We were able to correlate a band at 1170 cm^{-1} to platelet precipitates and three bands at 1040, 1060 and 1080 cm^{-1} to spheroidal precipitates in general agreement with previous attributions. More specifically, the band at 1040 cm^{-1} was correlated with a structure more close to a spherical precipitate morphology, the band at 1060 cm^{-1} more close to an octahedral morphology and the band at 1080 cm^{-1} more close to a polyhedral morphology. Additionally, it was found that in C containing irradiated material the production of the platelet precipitates is enhanced and the production of the spheroidal ones is reduced, although in (C, Sn) co-doped irradiated material the opposite behavior was observed. We have suggested that in the case of C containing Si the formed nucleation sites favor the formation of platelet precipitates, although in the case of (C, Sn) co-doped Si the enhanced formation of the nucleation sites cause an increase of the interfacial energy of the precipitates which favors spheroidal morphologies. Furthermore, the study of the evolution curve of C shows a partial recovery prior to the beginning of its complete disappearance. The phenomenon was attributed to the release of C atoms from $C_N(Si_I)_M$ complexes. In the case of (C, Sn) co-doping when the Sn concentration is relatively low, the recovery stage is enhanced in comparison with C-containing Si. The role of Sn as a temporarily trap of V, leading finally to an additional release of C, has been considered as a plausible explanation of the phenomenon. Nevertheless, when the Sn concentration is high, the recovery stage of C substitutional atoms is partially suppressed. Due to the enhanced strain in the Si lattice, the release of V from the transient SnV pairs is affected, leading in essence in a reduction of the annihilation rate between V and Si_I. Consequently, the recovery of C substitutional atoms is suppressed. Importantly, advances in the knowledge of the mechanisms that isovalent dopants, in particular Sn here, impact the O and C precipitation processes leads to a better understanding of the various interactions between the defects involved in the above processes and to the fabrication of improved devices.

Acknowledgements T. Angeletos is grateful to the A.S. Onassis Foundation for financial support through his PhD scholarship (Grant No. G ZL 001–1/2015–2016). The authors are grateful to Prof. H. Ohyama (Kumamoto National College of Technology, Japan) for the electron irradiations and Profs Neimash and Yamanaka for the provision of the Cz-Si:C,Sn_L and the Cz-Si:C,Sn_H sample, respectively.

Open Access This article is distributed under the terms of the Creative Commons Attribution 4.0 International License (http://creativecommons.org/licenses/by/4.0/), which permits unrestricted use, distribution, and reproduction in any medium, provided you give appropriate credit to the original author(s) and the source, provide a link to the Creative Commons license, and indicate if changes were made.

References

1. S.G. Cloutier, P.A. Kossyrev, J. Xu, Nat. Mater. **4**, 877 (2005)
2. E.N. Sgourou, D. Timerkaeva, C.A. Londos, D. Aliprantis, A. Chroneos, D. Caliste, P. Pochet, J. Appl. Phys. **113**, 113506 (2013)
3. H. Chroneos, R.W.G. Bracht, B.P. Uberuaga, Mater. Sci. Eng. B **154–155**, 72 (2008)
4. A. Chroneos, C. A. Londos, J. Appl. Phys. **107**, 093518 (2010)
5. H. Wang, A. Chroneos, C.A. Londos, E.N. Sgourou, U. Schwingenschlogl. Appl. Phys. Lett. **103**, 052101 (2013)
6. L.I. Murin, E.A. Tolkachava, V.P. Markevich, A.R. Peaker, B. Hamilton, E. Monakhov, B.G. Svensson, J.L. Lindström, P. Santos, J. Coutinho, A. Carvalho, Appl. Phys. Lett. **98**, 182101 (2011)
7. A. Chroneos, R.W. Grimes, H. Bracht, J. Appl. Phys. **105**, 016102 (2009)
8. A. Chroneos, C. Skarlatos, C. Tsamis, A. Christofi, D.S. McPhail, R. Huang, Mater. Sci. Semicond. Proc. **9**, 640 (2006)
9. R. C. Newman, R. Jones, in *Oxygen in Silicon, Semiconductors and Semimetals*, vol. **42**, ed. by F. Shimura (Academic Press, Orlando, 1994), p. 289
10. H. Bender, J. Vanhellemont, in *Handbook on Semiconductors, Materials, Properties and Preparations*, vol. **3b**, ed. by T.S. Moss, S. Mahajan (Elsevier, North-Holland, Amsterdam, 1994), p. 1637
11. A. Borghesi, B. Pivac, A. Sassella, A. Stella, J. Appl. Phys **77**, 4169 (1995)
12. G. Davies, R.C. Newman, in *Handbook on Semiconductors, Materials, Properties and Preparations*, vol. **3b**, ed. by T.S. Moss, S. Mahajan (Elsevier, North-Holland, Amsterdam, 1994), p. 1557
13. C.A. Londos, M.S. Potsidi, V.V. Emtsev, Phys. Stat. Solidi C **2**, 1963 (2005)
14. W. Scorupa, R.A. Yankov, Mater. Chem. Phys. **44**, 101 (1996)
15. G.D. Watkins, J.W. Corbett, Phys. Rev. **138**, A543 (1965)
16. T. Hallberg, J.L. Lindström, J. Appl. Phys. **72**, 5130 (1992)
17. C. Cui, D. Yang, X. Ma, R. Fan, D. Que, Phys. Stat. Solidi A **202**, 2442 (2005)
18. I. Yonenaga, T. Taishi, K. Inoue, R. Gotoh, K. Kutsukake, Y. Tokumoto, Y. Ohno, J. Cryst. Growth **395**, 94 (2014)

19. Y.V. Pomozov, M.G. Sosnin, L.I. Khirunenko, V.I. Yashnik, Semiconductors **34**, 994 (2000)
20. X. Xhu, Yu, D. Yang, J. Cryst. Growth **401**, 141 (2014)
21. X. Yu, J. Chen, X. Ma, D. Yang, Mater. Sci. Eng. R **74**, 1 (2013)
22. J. Vanhellemont, X. Zhang, W. Xu, J. Chen, X. Ma, D. Yang, J. Appl. Phys **108**, 123501 (2010)
23. J. Vanhellemont, M. Suezawa, I. Yonenaga, J. Appl. Phys **108**, 016105 (2010)
24. K. Sumino, I. Yonenaga, in *Oxygen in Silicon, Semiconductors and Semimetals*, vol. **42**, ed. by F. Shimura (Academic Press, Orlando, 1994), p. 450
25. H. Tsuya, in *Oxygen in Silicon, Semiconductors and Semimetals*, vol. **42**, ed. by F. Shimura (Academic Press, Orlando, 1994), p. 619
26. A. Chroneos, E.N. Sgourou, C.A. Londos, U. Schwingenschlögl, Appl. Phys. Rev. **2**, 021306 (2015)
27. H. Shimura, Tsuya, T. Kawamura, J. Appl. Phys. **51**, 269 (1980)
28. C. Claeys, E. Simoen, V.B. Neimash, A. Kraitchinskii, M. Krasko, O. Puzenko, A. Blondeel, P. Clauws, J. Electrochem. Soc. **148**, G738 (2001)
29. J.D. Murphy, K. Bothe, M. Olmo, V.V. Voronkov, R.J. Falster, ECS Trans. **33**, 121 (2010)
30. M. Akatsuka, K. Sueoka, N. Adachi, N. Morimoto, H. Katahama, Microelectron. Eng. **56**, 99 (2001)
31. K.F. Kelton, Phil. Trans. R. Soc. Lond. A **361**, 429 (2003)
32. O.De.. Gryse, P. Clauws, J. Van. Landuyt, O. Lebedev, C. Claeys, E. Simoen, J. Vanhellemont, J. Appl. Phys. **91**, 2493 (2002)
33. P. Gaworzewski, E. Hild, F.-G. Kirscht, L. Vecsernyes, Phys. Stat. Solidi A **85**, 133 (1984)
34. K. Tempelhhoff, F. Spiegelberg, R. Gleichmann, D. Wruck, Phys. Stat. Solidi A **56**, 213 (1979)
35. U. Gösele, MRS **59**, 419 (1986)
36. J.-Y. Huh, U. Gösele, T.Y. Tan, J. Appl. Phys. **78**, 5926 (1995)
37. P. Liu, X. Ma, J. Zhang, L. Liand, D. Que, J. Appl. Phys. **87**, 3669 (2000)
38. R.F. Hafer, T.S. Moss, Semicond. Sci. Technol. **22**, 179 (2007)
39. R. Romanyak, V. Melnic, V. Babich, V. Kladko, O. Gudymenko, V. Ilchenko, L. Lasyliev, A. Goriachko, Nanoscale Res. Lett. **9**, 693 (2014)
40. G.D. Watkins, J.W. Corbett, Phys. Rev. **121**, 1001 (1961)
41. L.I. Murin, J.L. Lindström, B.G. Svensson, V.P. Markevich, A.R. Peaker, C.A. Londos, Solid State Phenom. **108–109**, 267 (2005)
42. N.V. Sarlis, C.A. Londos, L.G. Fytros, J. Appl. Phys. **81**, 1645 (1997)
43. C.A. Londos, M. Potsidi, E. Stakakis, Physica B **340–342**, 551 (2003)
44. H. Wang, A. Chroneos, C.A. Londos, E.N. Sgourou, U. Schwingenschlögl, Sci. Rep. **4**, 4909 (2014)
45. R.C. Newman, J. Phys. **12**, R335 (2000)
46. K. Sueoka, E. Kamiyama, P. Spiewak, J. Vanhellemont, J. Solid State Sci. Technol. **5**, P3176 (2016)
47. V.V. Voronkov, R. Falster, Solid State Phenom. **178–179**, 3 (2011)
48. V.V. Voronkov, R. Falster, J. Appl. Phys **91**, 5802 (2002)
49. V.V. Voronkov, R. Falster, J. Electrochem. Soc **149**, G167 (2002)
50. A. Brelot, IEEE Trans. Nucl. Sci. **19**, 220 (1972)
51. A. Chroneos, C.A. Londos, E.N. Sgourou, J. Appl. Phys. **110**, 093507 (2011)
52. G.D. Watkins, Phys. Rev. B **12**, 4383 (1975)
53. E. Simoen, C. Claeys, V. Privitera, S. Coffa, M. Kokkoris, E. Kossionides, G. Fanourakis, A. Nylandsted Larsen, P. Clauws, Nucl. Instrum. Meth. Phys. Res. B **186**, 19 (2002)
54. F. Lemeilleur, G. Linström, S. Watts, 2nd RD48 status report. CERN/LHCC Rep. **98–39**, 1 (1998)
55. G. Linström, M. Moll, E. Fretwurst, Nucl. Istrum. Meth. Phys. Res. A **426**, 1 (1999)
56. T. Angeletos, E.N. Sgourou, A. Andrianakis, A. Diamantopoulou, A. Chroneos, C.A. Londos, J. Appl. Phys. **118**, 015704 (2015)
57. V.B. Neimash, A. Kraitchinskii, M. Kras'ko, O. Puzenko, C. Claeys, E. Simoen, B. Svensson, A. Kuznetsov, J. Electrochem. Soc. **147**, 7227 (2000)
58. L.I. Khirunenko, Y.V. Pomozov, M.G. Sosnin, Solid State Phenom. **82–84**, 111 (2002)
59. W. Wijaranakula, J. Appl. Phys. **69**, 2737 (1991)
60. W. Wijaranakula, J. Appl. Phys. **72**, 2713 (1992)
61. K. Sueoka, E.E. Kamiyama, P. Spiewak, J. Vanhellemont, ECS J. Solid State Sci. Technol. **5**, P3176 (2015)
62. A. Carvalho, R. Jones, Silicon, Germanium, and Their Alloys-Growth, Defects, Impurities and Nanocrystals, Chap. 4, (CRC Press, Boca Raton, 2014)
63. E. Kamiyama, K. Sueoka, J. Vanhellemont, Silicon, Germanium, and Their Alloys-Growth, Defects, Impurities and Nanocrystals, Chap. 5, (CRC Press, Boca Raton, 2014)
64. K. Sueoka, N. Ikeda, T. Yamamoto, S. Kobayashi. J. Appl. Phys. **74**, 5437 (1993)
65. U. Gösele, P. Laveant, N. Engler, P. Werner, MRS **610**, B7.1.1 (2000)
66. R. Pinacho, P. Castrillo, M. jaraiz, I. Martin-Bragado, J. Barbola, H.-J. Gossmann, G.-H. Gilmer, J.L. Benton, J. Appl. Phys. **92**, 1582 (2002)
67. S. Mirabella, A. Coati, D. De Salvador, E. Napolitani, A. Matoni, G. Bisognin, M. Berti, A. Carnera, A.V. Drigo, S. Scalese, S. Pulvirenti, A. Terrasi, F. Priolo, Phys. Rev. B **65**, 045209 (2002)
68. V.V. Emtsev, Jr., C.A.J. Ammerlaan, V.V. Emtsev, G.A. Oganesyan, B.A. Andreev, D.F. Kuritsin, A. Misiuk, B. Surma, C.A. Londos, Phys. Stat. Solidi B **235**, 75 (2003)
69. A. Misiuk, J. Bac Misiuk, A. Barch, A. Romano, M. Rodriguez, I.V. Antonova, V.P. Popov, C.A. Londos, J. Jun, Int. J. Hydrogen Energy **26**, 483 (2001)
70. V.V. Voronkov, Private communication
71. A. Borghesi, A. Sassella, P. Geranzani, M. Porrini, B. Pivac, Mat. Sci. Eng. B **73**, 145 (2000)
72. A. Sassella, A. Borghesi, G. Borionetti, P. Geranzani, Mater. Sci. Eng. **B 73**, 224 (2000)
73. D. Kot, G. Kissinger, M.A Schubert, A. Sattler, ECS J Sol. State Sci. Technol. **3**, P370 (2014)
74. T. Halberg, J.L. Lindstrom, J. Appl. Phys **72**, 5130 (1992)
75. Q. Ma, Y. Li, S. Yang, H. Liu, Q. Hao, Mater. Sci. Eng. B **122**, 218 (2005)
76. Q.-Y. Ma, Y.-X. Li, G.-F. Chen, S. Yang, L.-L. Liu, P.-J. Niu, D.-N. Chen, H.-T. Li, Chin. Phys. **14**, 1882 (2015)
77. S.M. Hu, J. Appl. Phys **51**, 5945 (1980)
78. A. Sassella, A. Borghesi, P. Geranzani, G. Borionetti, Appl. Phys. Lett. **75**, 1131 (1999)
79. V.V. Voronkov, R. Falster. J. Appl. Phys. **89**, 5965 (2001)
80. J. D. Eshelby, Proc. R. Soc. Lond. A **241**, 376 (1957)
81. F.M. Livingston, S. Messoloras, R.C. Newman, B.C. Pike, R.J. Stewart, N.J. Binns, W.P. Brown, J.G. Wilkes, J. Phys. C **17**, 6253 (1984)
82. J. Cheung, S. Messoloras, S. Rycroft, R.J. Stewart, M.J. Binns, Semicond. Sci. Technol. **15**, 782–788 (2000)
83. K. Wada, H. Nakanishi, H. Takaoka, N. Innoue, J. Cryst. Growth **57**, 535 (1982)
84. K. Wada, N. Innoue, K. Kohra, J. Cryst. Growth **49**, 479 (1980)
85. K. Sueoka, M Akatsuka, M. Yonemura, T. Ono, E. Asayama, Y. Koike, S. Sadamitsu, Solid State Phenom. **82–84**, 49 (2002)

86. F.S. Ham, J. Phys. Chem. Solids **6**, 335 (1958)
87. C.Y. Kung, J. Appl. Phys. **65**, 4654 (1989)
88. D. Kot, G. Kissinger, M.A. Schubert, M. Klingsporn, A. Huber, A. Sattler, Phys. Status Solidi RRL **9**, 405 (2015)
89. F. Zeller, C. Wurtser, K. Laβmann, W. Eisenmenger, Mater. Sci. Forum **258–263**, 399 (1997)
90. C.Y. Kung, Jpn. J. Appl. Phys. **31**, 2846 (1992)
91. D. Kot, G. Kissinger, M.A. Schubert, M. Klingsporn, A. Sattler, J. Solid States Sci. Technol. **3**, 370 (2014)
92. H. Fujimory, J. Electrochem. Soc. **144**, 9 (1997)
93. S. Zhang, M. Juel, E. J. Ovrelid, G. Tranell, J. Gryst. Growth **411**, 63 (2015)
94. S. Hahn, M. Arst, K.N. Ritz, S. Shatas, H.J. Stein, Z.U. Rek, W.A. Tiller, J. Appl. Phys. **64**, 849 (1988)
95. H.L. Tsai, in *Semiconductor Silicon 1986*, ed. by H.R. Huff, T. Abe, B. Kolbesen (The Electrochemical Society, Pennington, 1986), p. 790
96. S. Kishino, Y. Matsushita, M. Kanamori, T. Iizuka, Jpn. J. Appl. Phys. **21**, 1 (1982)
97. J.P.N.N. Nagasima, J. Appl. Phys **9**, 879 (1970)
98. D. Kot, Influence of vacancies introduced by RTA on the nucleation, size, morphology, and gettering efficiency of oxygen precipitates in silicon wafers, PhD Thesis, Brandenburg University of Technology Cottbus-Senftenberg (2013)
99. L.I. Murin, J.L. Lindstrom, V.P. Markevich, A. Misiuk, C.A. Londos, J. Phys. **17**, 2237 (2005)
100. O. De Gryse, P. Clauws, O. Lebedev, J. Van Landuyt, J. Vanhellemont, C. Claeys, E. Simoen, Physica B **308–310**, 294 (2001)
101. O. De Gryse, J. Vanhellemont, P. Clauws, O. Lebedev, J. Van Landuyt, E. Simoen, C. Claeys, Physica B **340–342**, 1003 (2003)
102. C.A. Londos, E.N. Sgourou, A. Chroneos, V.V. Emtsev. Semicond. Sci. Technol. **26**, 105024 (2011)
103. C.A. Londos, D. Aliprantis, E.N. Sgourou, A. Chroneos, P. Pochet, J. Appl. Phys **111**, 123508 (2012)
104. V.V. Voronkov, R. Falster, Phys. Stat. Solidi B **252**, 816 (2015)
105. J.L. Linström, H. Weman, G.S. Oehrlein, Phys. Stat. Solidi A **99**, 581 (1987)
106. K.A. Fukuoka, M. Honda, Jpn. J. Appl. Phys. **29**, 1625 (1990)
107. R. Bean, R.C. Newman, J. Phys. Chem. Solids **33**, 255 (1972)
108. C.A. Londos, E.N. Sgourou, A. Chroneos, J. Mater. Sci. Mater. Electron. **25**, 4872 (2014)
109. A. Chroneos, C.A. Londos, E.N. Sgourou, P. Pochet, Appl. Phys. Lett. **99**, 241901 (2011)
110. C.A. Londos, E.N. Sgourou, D. Hall, A. Chroneos, J. Mater. Sci. Mater. Electron. **25**, 2395 (2014)
111. V.B. Neimash, A. Kraitchinskii, M. Kras'ko, O. Puzenko, C. Claeys, E. Simoen, B. Svensson, A. Kuznetsov, J. Electrochem. Soc. **147**, 2727 (2000)
112. L.I. Khirunenko, O. Kobzar, Y.V. Pomozov, M.G. Sosnin, N.A. Tripachko, V.P. Markevich, L.I. Murin, A.R. Peaker, Phys. Stat. Solidi C **0**, 694 (2003)
113. C. Gao, X. Ma, J. Zhao, D. Yang, J. Appl. Phys **113**, 093511 (2013)
114. C. Gao, X. Ma, D. Yang, Phys. Stat. Solidi A **210**, 2199 (2013)
115. C. Claeys, J. Vanhellemont, Solid State Phenom. **6–7**, 21 (1989)
116. F. Shimura, J.P. Balardo, P. Fraundorf, Appl. Phys. Lett. **46**, 941 (1985)
117. F. Shimura, J. Appl. Phys. **59**, 3251 (1986)
118. C. Maddalon-Vinande, J.P. Vallard, D. Barbier, J. Electrochem. Soc. **142**, 2071 (1995)
119. A. Bourret, Mater. Res. Soc. 59, 223 (1986)
120. G. Kissinger, *Oxygen Precipitation in Silicon in Defects and Impurities in Si Materials*, ed. by Y. Yoshida, G. Langouche, (Springer, Berlin, 2015), p. 273
121. G. Kissinger, G. Dabrowski, A. Slatter, C. Serving, T. Muller, H. Richter, W. von Ammon, J. Electrochem. Soc. **154**, H454 (2007)
122. R. Falster, V.V. Voronkov, F. Quast, Phys. Stat. Solidi B **222**, 219 (2000)
123. K. Yasutake, M. Umeno, H. Kawabe, Phys. Stat. Solidi A **88**, 207 (1984)
124. G. Kissinger, J. Dabrowski, T. Sinno, Y. Yang, D. Kot, A. Sattler, J. Cryst. Growth. doi:10.1016/j.jcrysgro.2016.10.073
125. C.A. Londos, A. Andrianakis, V. Emtsev, H. Ohyama, J. Appl. Phys. **105**, 123508 (2009)
126. A. Mattoni, F. Bernardini, L. Colombo, Phys. Rev. B **66**, 195214 (2002)
127. S.S. Kapur, M. Prasad, T. Sinno, Phys. Rev. B **69**, 155214 (2004)
128. J.L. Hastings, S.K. Estreicher, P.A. Fedders, Phys. Rev. B **56**, 10215 (1999)
129. M. Prasad, T. Sinno, Phys. Rev. B **68**, 045206 (2003)
130. S.S. Kapur, T. Sinno, Phys. Rev. B **82**, 045205 (2010)
131. S. Lee, G.S. Hwang, Phys. Rev. B **78**, 045204 (2008)
132. P.W. Atkins, *Physical Chemistry*. (Oxford University Press, Oxford, 1994)